Enhancing the ferroelectric performance of P(VDF-co-TrFE) through modulation of crystallinity and polymorphism

Spampinato, Nicoletta; Maiz, Jon; Portale, Giuseppe; Maglione, Mario; Hadziioannou, Georges; Pavlopoulou, Eleni

Published in:
Polymer

DOI:
10.1016/j.polymer.2018.06.072

Publication date:
2018

Polymer 149 (2018) 66–72

Contents lists available at ScienceDirect

Polymer

journal homepage: www.elsevier.com/locate/polymer

Enhancing the ferroelectric performance of P(VDF-co-TrFE) through modulation of crystallinity and polymorphism

Nicoletta Spampinato [a], Jon Maiz [a, 1], Giuseppe Portale [b], Mario Maglione [c], Georges Hadziioannou [a], Eleni Pavlopoulou [a, *]

[a] Laboratoire de Chimie des Polymères Organiques (LCPO - UMR 5629), Bordeaux INP, Université de Bordeaux, CNRS, 16 Av. Pey-Berland, 33607, Pessac, France
[b] Zernike Institute for Advanced Materials, University of Groningen, Nijenborgh 4, NL-9747 AG, Groningen, the Netherlands
[c] Institut de Chimie de la Matière Condensée de Bordeaux, (ICMCB-UPR9048), CNRS, 87 Av. Dr Schweitzer, 33608, Pessac, France

ARTICLE INFO

Article history:
Received 12 March 2018
Received in revised form
8 June 2018
Accepted 25 June 2018
Available online 26 June 2018

Keywords:
Ferroelectric polymers
P(vdf-trfe)
Processing
Structure-function relations
Giwaxs

ABSTRACT

The functional properties of P(VDF-*co*-TrFE) are strongly dependent on its structure, which, in turn, depends on processing conditions applied. In this work we investigate the P(VDF-*co*-TrFE) processing-structure-function relationships, in order to find the thermal conditions that result in optimum ferroelectric performance in thin film configuration. Our results show that annealing temperature affects mostly the remnant polarization value, P_r, while annealing time has a severe effect on the coercive field, E_c. An optimized ferroelectric functionality, in terms of high P_r of about 90 mC/m^2 and low E_c of 50 MV/m, is achieved and rationalized through structural analysis by means of GIWAXS. The best performing structure exhibits a high degree of crystallinity, a preferential orientation of the crystallites with the polymer chains parallel to the substrate and the occurrence of three ferroelectric phases. A deconvolution study demonstrates the presence of a moderately unstable ferroelectric phase that is designated to facilitate ferroelectric switching. Our findings show that a single step of 15 min annealing at 135 °C leads to high performance P(VDF-*co*-TrFE) structure, proving that the 2 h-long annealing step that is traditionally applied is not necessary.

1. Introduction

Thanks to the emergence of organic electronics, ferroelectric polymers are nowadays experiencing their second blossom. After being used for decades in acoustic and electromechanical applications (e.g. microphones, sensors, pressure switches, etc.) [1] poly (vinylidene fluoride) (PVDF) and its copolymers with trifluoroethylene (P(VDF-*co*-TrFE)), are now incorporated in modern nano-sized electronic devices, expanding their conventional functionalities, thanks to the merits brought by the electroactive nature of these materials. Their functionality combined with the intrinsic advantages of polymers (i.e. solution process-ability, flexibility, lightness, low cost) enables their integration in organic electronic devices such as ferroelectric field effect transistors [2] or data storage devices [3–5].

In most devices the ferroelectric polymer is used in form of a thin film. In order to enhance the performance of the device, the functionality brought by the ferroelectric layer should be optimized. In particular the ferroelectric performance of P(VDF-*co*-TrFE) is known to depend on its structure. Structure, in turns, can be tuned through film processing. Although a thorough investigation of the structure and crystallization properties of bulk P(VDF-*co*-TrFE) has been attempted in literature since the 80's [6–16], studies that relate film processing conditions to the final ferroelectric or piezoelectric properties are rare [17–24] and concern only the effect of annealing temperature or casting solvent. Due to the lack of processing-function correlations, one can find in literature several annealing conditions for the processing of P(VDF-*co*-TrFE). Just to mention a few, annealing temperatures of 120 °C [25], 130 °C [22], 135 °C [12,16,26], 140 °C [27,28], have been applied during various annealing times such as 30 min [22], 1 h [21,29], 2 h [27,30,31], 5 h [32], 8 h [18], 12 h [12,13,31], or even 24 h [25]. The choice of

* Corresponding author.
E-mail address: epavlopoulou@enscbp.fr (E. Pavlopoulou).
[1] Present Address: POLYMAT and Polymer Science and Technology Department, University of the Basque Country (UPV/EHU), Paseo Manuel de Lardizabal 3, Donostia-San Sebastian, 20018, Spain.

https://doi.org/10.1016/j.polymer.2018.06.072
0032-3861/

annealing conditions seems arbitrary and mostly depends on empirical observations. This stresses the need for dedicated studies that investigate the link between processing conditions, resulting structure and final ferroelectric properties. Such studies are an indispensable tool for exploiting the utmost of the functional properties of P(VDF-*co*-TrFE) films.

The processing method that is commonly used for ferroelectric films incorporated in electronic devices comprises the annealing of a spin-cast film on a hot plate and its subsequent cooling. This method induces the cold-crystallization of the P(VDF-*co*-TrFE) films, i.e. the low-crystallinity spin-cast films are allowed to further crystallize upon annealing. Given the intrinsic link between polarization and dipoles orientation within the P(VDF-*co*-TrFE) crystallites [1], triggering the crystalline structure that is induced during cold-crystallization and cooling is expected to affect ferroelectric properties. Annealing temperature and annealing time can be used as levers for varying the cold-crystallization conditions and, subsequently, for enhancing crystallinity and ferroelectric performance in P(VDF-*co*-TrFE) films.

Herein, an integrated study of the processing-structure-function relationships that dictate the ferroelectric performance of P(VDF-*co*-TrFE) is conducted. To comply with the needs of electronic devices fabrication, thin films are studied, as opposed to bulk P(VDF-*co*-TrFE) that has been commonly investigated in literature. The cold-crystallization of these films is explored for various annealing temperatures and times that range between 130 °C and 140 °C and between 0 s (i.e. no annealing) and 2 h respectively. The crystalline structure of the cold-crystallized P(VDF-*co*-TrFE) films is investigated by means of grazing incidence wide angle x-ray scattering (GIWAXS), which provides additional information on the films' texture, while the ferroelectric properties are determined by recording the polarization *versus* electric field hysteresis loops of P(VDF-*co*-TrFE) simple capacitors. The annealing temperature and time are shown to impact the remnant polarization and the coercive field, respectively. The processing conditions that result in the most performing ferroelectric films are identified and rationalized through a thorough analysis of their structure.

2. Experimental section

2.1. Materials and samples preparation

The random copolymer P(VDF-*co*-TrFE) (with a 75/25 VDF/TrFE molar ratio) was provided by courtesy of Piezotech® FC (France). Cyclopentanone (SIGMA-Aldrich) was used as received without any further purification.

A solution containing 10 wt% of P(VDF-*co*-TrFE) in cyclopentanone has been prepared and spin-coated on Si substrates (for GIWAXS) or on Al/glass substrates (for capacitors). The films were heated on a precision hot plate with a rate of 5 °C/min starting from room temperature until the temperature of choice (130 °C, 133 °C, 135 °C, 137 °C, 140 °C). The temperature range explored is set between the crystallization temperature, T_c, and the melting temperature, T_m, because in this range an enhanced degree of crystallinity, driven by the rearrangement of molecular chains [29], is induced. T_c and T_m were determined by DSC scans performed on P(VDF-*co*-TrFE) powder (Fig. S1, Supplementary Data). Already during this heating ramp the cold-crystallization of the films is initiated, as proven by the exothermic peak that follows the Curie transition shown in the DSC scans of a self-standing film (Fig. S2, Supplementary Data). Then an isothermal annealing step is conducted at the selected temperature for 5 min, 15 min, 30 min, 1 h or 2 h, during which cold-crystallization continues. Finally, the films were let to cool down to room temperature slowly, with a cooling rate of 1.6 °C/min on the same hot stage. Additionally, a pristine film (i.e. not thermally treated) has been studied and used as a reference sample. The thickness of all films is 1 μm as measured by profilometry (BRUKER DEKTAK XT-A). Any cyclopentanone solvent residuals that may have remained trapped in the films are eliminated during the cold crystallization step. Among all different combinations of annealing temperatures and times tested, we opt to present in this manuscript two series of samples that are representative of the effect of temperature and of the effect of annealing time.

2.2. Capacitor fabrication

Aluminum electrodes were thermally evaporated onto clean glass substrates to form 100 nm thick bottom electrodes (ME400B PLASSYS evaporator) that were subsequently coated with the P(VDF-*co*-TrFE) films. 100 nm thick top Al electrodes were finally thermally evaporated. The temperature inside the evaporator was kept below 70 °C, i.e. below the Curie transition temperature, to avoid undergoing the ferroelectric-to-paraelectric transition. The thermal treatment of P(VDF-*co*-TrFE) has been conducted on the devices (i.e. after top electrode deposition) following the procedure described above.

2.3. Characterizations

Thermal Analysis. DSC curves were obtained using a TA Instrument DSC Q100 RCS. The DSC analysis has been performed *a)* on P(VDF-*co*-TrFE) 75/25 powder from room temperature to 200 °C at a heating/cooling rate of 10 °C/min and *b)* on free standing films prepared by drop-casting. Concerning the powder sample, a first heating ramp was used to erase thermal history, however, herein we present the first cooling and the second heating ramps, in consistence with common practice. Concerning the free standing samples, they were heated in the DSC crucible from room temperature until the respective crystallization temperature with a rate of 5 °C/min. Then an isothermal step has been conducted at the crystallization temperature for 15 min, and then a cooling ramp has been performed with a rate of 1.6 °C/min, until room temperature. This sequence mimics the preparation conditions used for the films under study. The heating and cooling rates correspond to those of the hot plate used for thermal processing. Right after, a second heating cycle has been performed from room temperature to 200 °C at a rate of 10 °C/min. The DSC curves presented in the main text have been recorded during the second heating ramp.

Ferroelectric measurements. Polarization hysteresis loops of the metal/ferroelectric/metal capacitors have been recorded at room temperature using the TF Analyzer 2000E of aixACCT Systems. A continuous sinusoidal wave with a 0.1 Hz frequency has been used and a 150 MV/m electric field was applied to ensure that saturation is reached. 8 devices have been measured per sample and a statistical study has been performed in order to corroborate the reproducibility of the polarization loops and to evaluate the associated error bars.

Structural characterization by means of GIWAXS. For GIWAXS measurements, the P(VDF-*co*-TrFE) films were spin-coated on silicon substrates following the same preparation and processing conditions used for the capacitors. The GIWAXS experiments have been performed at the Dutch-Belgian beamline (DUBBLE CRG, station BM26B) of the European Synchrotron Radiation Facility (ESRF) in Grenoble, France [33]. X-rays photons with 12 keV energy were used and the sample-to-detector distance was set at 8 cm. The angle of incidence α_i was set at 0.15°, slightly above the polymer critical angle to allow full penetration of the polymer film. The diffracted intensity was recorded by a Frelon CCD camera and was normalized by the incident photon flux and the acquisition time (30 s). Flat field, polarization, solid angle and efficiency corrections

were subsequently applied to the 2D GIWAXS images [34]. The scattering vector q was defined with respect to the center of the incident beam and has a magnitude of $q = (4\pi/\lambda)\sin(\theta)$, where 2θ is the scattering angle and λ is the wavelength of the x-ray beam (here $\lambda = 1.033$ Å). We opted to present the wedge-shaped corrected images where q_r and q_z are the in-plane and near out-of-plane scattering vectors, respectively. The scattering vectors are defined as follows: $q_x = (2\pi/\lambda)$ (cos $(2\theta_f)$cos (α_f)-cos (α_i)), $q_y = (2\pi/\lambda)$ (sin $(2\theta_f)$cos (α_f)), $q_z = (2\pi/\lambda)$ (sin (α_f)+sin (α_i)), $q_r^2 = q_x^2 + q_y^2$, and $q^2 = q_r^2 + q_z^2$, where α_f is the exit angle in the vertical direction and $2\theta_f$ is the in-plane scattering angle, in agreement with standard GIWAXS notation [35].

3. Results and discussion

Depending on thermal processing conditions, the ferroelectric properties of P(VDF-*co*-TrFE) films change significantly. Fig. 1a presents the polarization *vs* electric field (*P vs E*) hysteresis loops recorded by applying an external electric field of 150 MV/m under a frequency of 0.1 Hz for the P(VDF-*co*-TrFE) films isothermally annealed at various crystallization temperatures (T-130, T-133, T-135, T-137, T-140) during a fixed time of 15 min. The response of the not annealed (pristine) film with respect to the annealed ones clearly shows the drastic overall effect of thermal treatment: an enhanced ferroelectric response is achieved after annealing. The remnant polarization, P_r, almost doubles (from 38 mC/m^2 for the not annealed to 70 mC/m^2 for T-130) while the coercive field, E_c, reduces to half (from 96 MV/m for the not annealed to 56 MV/m for T-130). Concerning the annealed devices, samples T-130 and T-140 exhibit lower P_r compared to samples T-133, T-135 and T-137 that were annealed at temperatures close to the crystallization onset (Fig. 3a). Those latter exhibit a very high P_r, almost 90 mC/m^2. E_c value is only mildly dependent on annealing temperature, it is lower than 57 MV/m for all annealed samples and it exhibits a minimum of 50 MV/m for sample T-135. Fig. 1b presents the corresponding electric current *vs* electric field (*I vs E*) curves. Sharper switching current peaks are recorded for T-133 and T-135, which suggest a faster ferroelectric switching. We thus conclude that T-135 exhibits the best ferroelectric response in terms of faster switching rate, lower E_c (50 MV/m), higher P_r (89 mC/m^2). Hence, this temperature has been chosen to show the effect of annealing time on ferroelectric properties.

Fig. 2a presents the hysteresis loops obtained for the samples isothermally crystallized at 135 °C during various annealing times, between 0 s and 120 min (i.e. pristine film, t-5, t-15, t-30, t-60, t-120). Annealing for just 5 min already results in a decrease of E_c from 96 MV/m for the pristine film to 78 MV/m, which further decreases to 50 MV/m for samples annealed for 15 min (t-15) and 30 min (t-30) (Fig. 3b). This is the lowest electric field for the ferroelectric switching process. However, increasing annealing time above 30 min results in increasing E_c. In consistence with this observation, the corresponding switching current peaks are significantly shifted along the electric field axis (Fig. 2b). The sharper ones are centered at the lowest E_c and correspond to samples t-15 and t-30. As far as P_r is concerned, no trend is observed. A 5 min annealing already results in a high P_r value of 82 mC/m^2 close to the maximum P_r obtained for t-15.

Two main conclusions can be derived from these experiments. First, annealing temperature mostly affects remnant polarization, while annealing time has more influence on coercive field. Fig. 3a and b respectively show the effect of temperature on P_r and the effect of time on E_c, as these were discussed above. This result already provides a tool for tuning ferroelectric properties through processing. When one seeks to increase the surface charge density – and thus the amount of information stored in a device – annealing temperature should be modulated. On the other hand, if promoting a fast ferroelectric switching is the objective, one should tune the annealing time.

The second conclusion concerns the processing conditions that should be applied for optimum ferroelectric performance. The shaded areas in Fig. 3a and b suggest that a maximum polarization and a minimum coercive field are achieved when the isothermal cold-crystallization step is performed in the temperature range between 133 °C and 137 °C for short annealing times of only 15 to 30 min. This processing conditions result not only in high P_r and low E_c but also in square hysteresis loops with minor polarization losses when passing from the saturated polarization P_s to the remnant value P_r, fast switching and, thus, very good bistability of the ferroelectric properties of the prepared devices. In fact, the result that optimum ferroelectric response is achieved for only 15 min of annealing is particularly interesting for industrial applications where time-consuming and energy-consuming treatments are not desirable. Here it is demonstrated that long annealing treatments are not necessary since they do not lead to a functional improvement but rather deteriorate device performances. We can conclude that the 2 h annealing step has been mostly used so far [27,30,31] can be replaced by a shorter and more efficient thermal treatment such as that dictated by our study.

In order to explore the origin of this enhanced ferroelectric performance under certain processing conditions, grazing incidence wide angle x-ray scattering (GIWAXS) experiments have been performed. This allows to identify and quantify the crystalline phases present in P(VDF-*co*-TrFE) films. It is stressed that due to the small thickness of the film under study and the preferential orientation of the crystallites induced by confinement, DSC experiments on these same films would not be possible and partial information would not be provided with respect to that included in the GIWAXS data. Films for GIWAXS have been deposited on Si

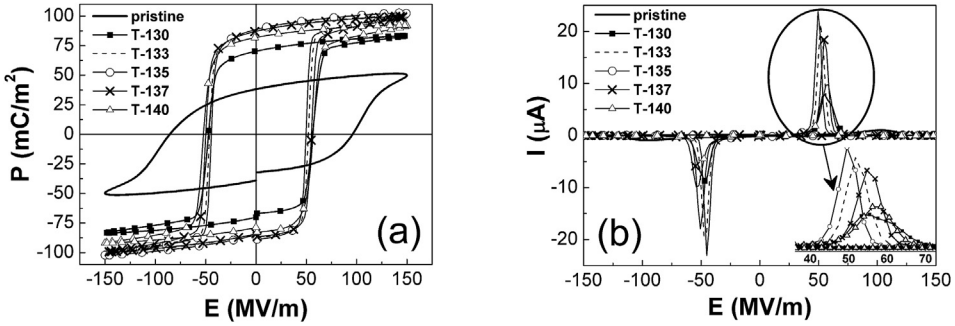

Fig. 1. (a) Polarization *vs* electric filed hysteresis loops for the pristine sample and for those annealed at 130 °C, 133 °C, 135 °C, 137 °C and 140 °C for 15 min, and (b) the corresponding current *vs* electric field data. The height of the symbols on the polarization curves corresponds to the error bar associated with the remnant polarization.

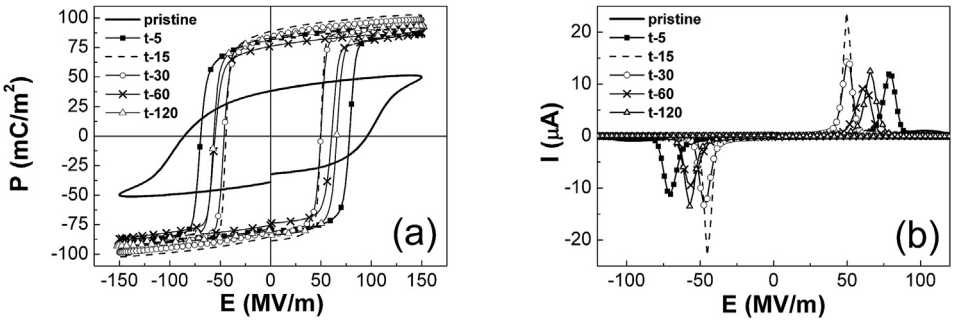

Fig. 2. (a) Polarization *vs* electric filed hysteresis loops for the pristine sample and for those annealed at 135 °C for 5 min, 15 min, 30 min, 60 min and 120 min (b) the corresponding current *vs* electric field data. The height of the symbols on the polarization curves corresponds to the error bar associated with the remnant polarization.

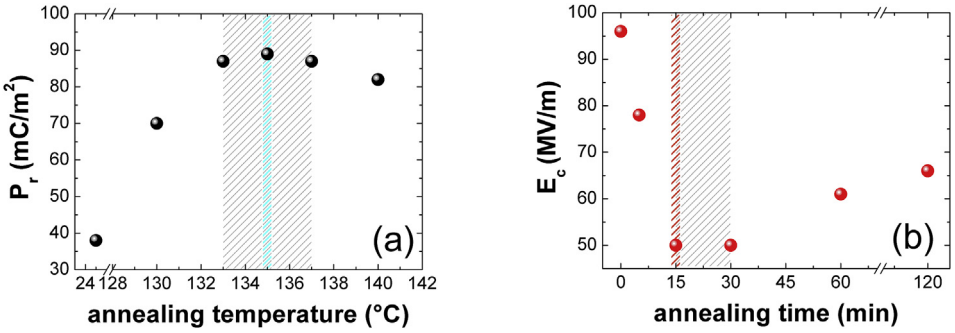

Fig. 3. (a) Effect of annealing temperature on P_r and, (b) effect of annealing time on E_c.

substrates following the same processing conditions as those followed for the fabrication of the capacitors. Si has been chosen instead of Al because it scatters less than Al. This is important for a quantitative analysis as the one endeavored below since all background contributions should be removed as precisely as possible. Nonetheless we have cross-checked that the orientation of the crystallites is not affected by the choice of the substrate. 2D scattering patterns have been recorded at room temperature for all films processed using the same thermal protocols studied above. All necessary corrections (listed in the Experimental Section) have been applied to the raw GIWAXS patterns, including background scattering subtraction and wedge correction [34]. The corrected 2D images were radially integrated to extract the 1D scattered intensity *vs* scattering vector (*Intensity vs q*) pattern. Fig. 4a shows the *Intensity vs q* scattering pattern obtained for the film that was annealed at 135 °C for 15 min while the corresponding wedge-corrected 2D image is presented in the inset. This pattern includes the typical reflections that are assigned to the ferroelectric orthorhombic unit cell of P(VDF-*co*-TrFE) [13,14,36,37]. The first peak at around 1.5 $Å^{-1}$ corresponds to a combination of the (200) and (110) reflections, the second peak at 2.6 $Å^{-1}$ to the superposition of (001), (310) and (020) planes, and the third one at 3 $Å^{-1}$ is assigned to the (111) and (201) reflections, which spatially overlap with the second order reflections (220) and (400). In the scattering image, the (110), (200) reflection appears more intense on the meridian, which is consistent with a preferential orientation of the *c*-axis (i.e. of the chain backbone) parallel to the substrate [30]. This crystal orientation favors ferroelectricity, since in P(VDF-*co*-TrFE) the dipoles that induce the ferroelectric property are perpendicular to the backbone and therefore in this case they are oriented parallel to the external applied electric field. All films under study exhibit this orientation, as apparent in Figs. S3 and S4 (Supplementary Data), except sample T-140 that will be discussed later on.

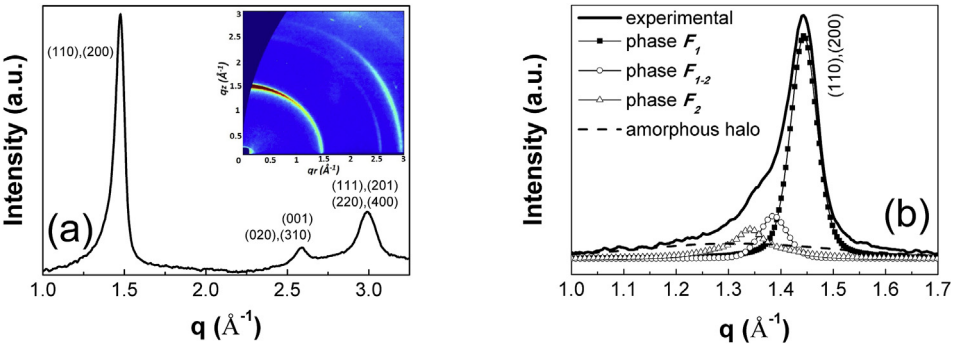

Fig. 4. a) The 1D GIWAXS pattern obtained for the films annealed at 135 °C for 15 min and the corresponding 2D wedge-corrected GIWAXS image (inset). b) A zoom at the (110), (200) peak, along with the fitted curves that were used to deconvolute this peak.

According to current understanding concerning the phase transitions in P(VDF-*co*-TrFE) [11–13,16,38–41], no paraelectric phase exists below the Curie temperature but only ferroelectric ones. In particular Kim et al. [12,13] and Gregorio et al. [40] examined the Curie transition mainly by DSC and concluded that several ferroelectric phases can co-exist at room temperature, having different amounts of conformational gauche defects and hence different thermodynamic stability. Moreover, gauche defects are reported to induce lattice expansion, which shifts the Bragg peak to lower angles [12–14]. Indeed, the presence of defects is expected to induce a less compact packing of chains, which results in an increased *d*-spacing along the *a* and *b* axes and consequently in a Bragg reflection that appears at lower *q*-values in the reciprocal space with respect to a less- or non-defective phase. This suggests that at room temperature each ferroelectric phase – characterized by a different amount of defects – crystallizes into an orthorhombic unit cell, with slightly different lattice parameters depending on the amount of defects. Based on this, the peak at around 1.5 $Å^{-1}$ should be considered as the superposition of the (110), (200) reflections of different ferroelectric phases. For the analysis carried out below we deconvolute this peak into the sum of an intense, predominant peak that is assigned to a ferroelectric phase with a low degree of gauche defects, named ***F1***, and a second less intense peak that is centered between 1.3 and 1.4 $Å^{-1}$ and is assigned to a more defective ferroelectric phase, named ***F2***. Note that several names have appeared in literature in the past to describe ferroelectric phases with different amount of defects [14,40,41]. For samples T-133, T-135 and t-30, an intermediate peak is present in our data, located between the peaks that are assigned to ***F1*** and ***F2*** phases. Deconvolution of these patterns absolutely necessitates the introduction of this third peak. We assign this peak to an additional ferroelectric phase, less ordered/more defective than ***F1*** but more ordered/less defective than ***F2***. Therefore we name this intermediate phase ***F1-2***. The position of this peak justifies the correlation made with the amount of defects.

The ***F1***, ***F2*** and ***F1-2*** peaks have been described by pseudo-Voigt functions. Additionally, a broad peak which extends from 0.7 $Å^{-1}$ to 1.6 $Å^{-1}$ should be considered and it is assigned to the amorphous halo contribution. To limit any possible error, a statistical study has been conducted (i.e. for every sample the deconvolution has been performed several times) while some parameters, such as the ***F1*** peak position (concerning the crystalline contribution) which is easily identified from the data, and the width of the amorphous halo (concerning the amorphous contribution), have been kept fixed. This latter is imposed by the shape of the halo measured for a molten film at 165 °C and fitted with an asymmetric function. The parameters that are related to the width of this asymmetric function have been kept fixed for deconvolution in order to correctly consider the shape of the amorphous halo [42]. The parameters related to the amplitude and to the position of the halo were free to vary. The deconvolution performed on sample T-135 is presented in Fig. 4b as an example. All the other deconvolutions are presented in Fig. S5, Supplementary Data. Although only the 1–1.7 $Å^{-1}$ *q*-range is presented in Fig. 4b for clarity reasons, deconvolution has been performed between 0.8 $Å^{-1}$ and 2 $Å^{-1}$.

Based on the deconvolution of the (110), (200) peak we can evaluate the degree of crystallinity, χ_{ferro}, and the amount of each ferroelectric phase in each sample. The degree of crystallinity we calculate is not the absolute one, but slightly lower than that, due to the missing scattered intensity for $0° < \chi < 5°$ (at $q \approx 1.5\ Å^{-1}$), χ being the polar angle, defined with respect to the out-of-plane direction. Thanks to the apparent amorphous halo contribution, the degree of crystallinity is calculated similarly to the case of WAXS, using Equation (1):

$$\chi_{ferro} = \frac{A_{F1} + A_{F2} + A_{F1-2}}{A_{tot}} \quad (1)$$

where A_{F1}, A_{F2}, and A_{F1-2} (when applicable) are the integrated areas of the respective fitted peak and A_{tot} is the total area of the (110), (200) peak, i.e. the sum the areas of the ferroelectric peaks plus the amorphous halo contribution. It is noted that since the films are studied below the Curie temperature, ferroelectric crystallinity corresponds to total crystallinity [40].

Fig. 5a and b show the evolution of the degree of crystallinity in these ferroelectric P(VDF-*co*-TrFE) films *versus* annealing time and annealing temperature. The shady parts correspond to the annealing conditions that result in the optimum ferroelectric performance. Clearly, the pristine sample (that corresponds to 0 annealing time in Fig. 5a and 25 °C in Fig. 5b) exhibits the lowest crystallinity and contains the highest amount of amorphous phase (see also Fig. S5, Supplementary Data). Moreover, the contribution of the defective ***F2*** crystalline phase dominates over that of the more ordered ***F1*** phase, as witnessed by its higher intensity and bigger area (Fig. S5). For the annealed samples the situation is reversed, and ***F1*** dominates over ***F2*** and ***F1-2***. Note that the ferroelectric response of the pristine film is very poor compared to that of the annealed films (Figs. 1a and 2a). This result is expected, since annealing is known to increase the degree of crystallinity, which consequently increases polarization [17,39] given that the crystalline domains are the only regions involved in the ferroelectric switching process which is accomplished by the rotations of individual dipoles around the chain axes [17].

Concerning the effect of annealing time Fig. 5a suggests that crystallinity increases rapidly within the first 15–30 min of annealing and then reaches a plateau at which the fraction of ferroelectric phase is considerably high, around 80%. This result asserts that it is not necessary to perform a long thermal treatment of 2 h in order to obtain a high degree of crystallinity, but only 15 or 30 min are enough, and, in fact, optimum device performance is achieved for these short times, as evidenced by the shady area.

Regarding the annealing temperature effect, we can assert that ferroelectric crystallinity increases with annealing temperature (Fig. 5b), in consistence with previous reports [17], and reaches its maximum value when annealing is performed at 140 °C. However, the GIWAXS image recorded for sample T-140 shows that an inversion of crystallite orientation has occurred at this temperature (Fig. S6, Supplementary Data). The (110), (200) ring is now more pronounced at the equatorial than in the meridian, implying that the majority of polymer chains are oriented with their backbone perpendicular to the substrate, and, consequently, the dipoles are not aligned parallel to the electric field direction. This inverted orientation has a negative impact on the ferroelectric response and justifies the decreased P_r, despite the high degree of crystallinity in T-140.

On the other hand, the highly-performing T-133, T-135 and t-30 samples exhibit a chain orientation parallel to the substrate, a high crystallinity and, moreover, the intermediate phase ***F1-2***. This intermediate state has some gauche defects, which are fewer than in case of phase ***F2***, and is considered to be a slightly unstable ferroelectric phase. We suggest that this phase is responsible for the superior ferroelectric performance of these films, given that the presence of some gauche defects in the ferroelectric crystal is reported to favor dipole rotation along the chain, by decreasing the respective potential energy barrier and facilitates polarization switching [13].

Finally, to further support the information derived by GIWAXS we present below DSC data recorded for self-standing films. As explained in the Experimental section, drop-casted films were

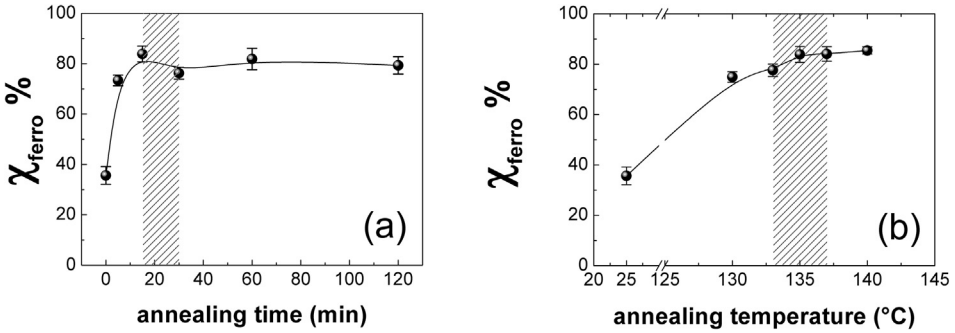

Fig. 5. Degree of ferroelectric crystallinity as a function of: (a) annealing time for a fixed annealing temperature 135 °C and (b) annealing temperature for a fixed annealing time 15 min. The lines that connect the data points serve as guides to the eye. The shady parts correspond to the annealing conditions that result in the optimum ferroelectric performance.

prepared and underwent in the DSC crucible the same thermal treatment performed for the cold-crystallization of the thin films, i.e. heating, isothermal annealing and cooling to room temperature with the same rates imposed by the hot plate. Right after, a second heating ramp has been performed from room temperature to 200 °C at a rate of 10 °C/min. The DSC curves recorded during this last ramp are presented in Fig. 6. A shift of the melting peak position towards higher temperatures is observed, which indeed indicates a better arrangement of the crystalline phase in bigger crystallites in case of semi-crystalline polymers [40]. T_m increases following the same trend obtained for the crystallinity (i.e., sample T-130 has a lower T_m with respect to T-133) and then T_m remains constant for samples T-133, T-135 and T-137, before increasing further for T-140. Conversely, the maximum of the Curie peak, T_{Curie}, slightly shifts towards lower temperatures when the annealing temperature is increased. This shift has already been correlated in literature with a larger amount of defects, since the generated ferroelectric phases require less energy in order to undergo the Curie transition [13]. Both the Curie transition peak and the melting peak correspond to a first order transition, but in case of the Curie transition the peak is broad indicating the participation of different ferroelectric phases to this transition [12,36]. Therefore the occurrence of the $\boldsymbol{F_2}$ and $\boldsymbol{F_{1\text{-}2}}$ ferroelectric phases, in addition to the less defective $\boldsymbol{F_1}$ phase is confirmed.

4. Conclusions

In this work the effect of thermal processing on the ferroelectric properties of P(VDF-*co*-TrFE) films has been studied and the conditions that result in the best performing films have been identified. The annealing temperature was varied between 130 °C and 140 °C and the annealing time varied between 0 s (i.e. no annealing) and 2 h. It is noted that, to the best of our knowledge, the effect of annealing time on the ferroelectric performance has not been studied so far and most usually annealing treatments as long as 2 h have been reported in literature. Our results suggest that only 15 min are enough to induce a high ferroelectric performance. In fact optimal ferroelectric response, in terms of a high P_r and a low E_c, has been achieved when thermal processing takes place in the temperature range between 133 °C and 137 °C for 15 to 30 min. Thus, a P_r as high as 89 mC/m^2 and an E_c as low as 50 MV/m have been obtained. Moreover it is shown that annealing temperature affects mostly the remnant polarization value, while annealing time has a severe effect on the coercive field value.

The enhanced performance achieved under these conditions has been rationalized through GIWAXS studies that revealed the crystalline phases apparent in these films and allowed the calculation of the degree of crystallinity. It is shown that a high degree of crystallinity is necessary for an improved performance, but this is not the only crucial parameter. An orientation of the crystallites with the *c*-axis parallel to the substrate is imperative. Moreover, the existence of an intermediate, slightly unstable, ferroelectric phase $\boldsymbol{F_{1\text{-}2}}$ that contains some gauche defects is shown to improve the ferroelectric performance by facilitating the rotation of dipoles during the ferroelectric switching. Our study shines light on the processing-structure-function relationships that dictate the performance of ferroelectric P(VDF-*co*-TrFE) films and provide the processing conditions that should be applied for the maximum exploitation of the ferroelectric functionality in organic electronic devices. Moreover, our results are of general interest considering the increasing insertion of P(VDF-*co*-TrFE) layers in organic electronic devices that exploit the functionalities added by the ferroelectric nature of this polymer.

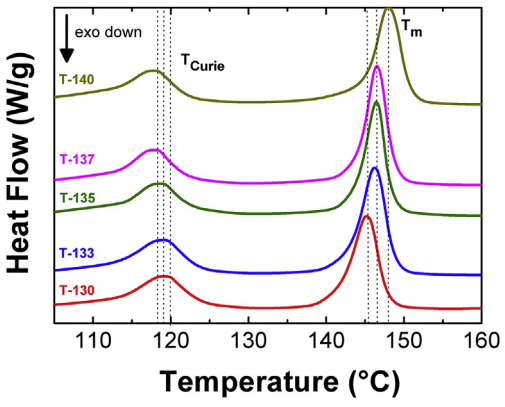

Fig. 6. DSC heat flow curves recorded for free standing P(VDF-*co*-TrFE) films upon the second heating cycle. The curves are presented shifted along the *y* axis for clarity.

Acknowledgements

This work was performed within the framework of the Labex AMADEus ANR-10-LABEX-0042-AMADEUS with the help of the French state Initiative d'Excellence IdEx ANR-10-IDEX-003-02. N.S. is grateful to the Labex AMADEus for financial support. J.M. acknowledges financial support from TOURS2015 project ("Investissements d'Avenir" Program of the French State) through the grant agreement n° O12590-401530. Financial support from the HOMERIC Industrial Chair (Arkema/ANR) with the grant agreement no AC-2013-365 is also acknowledged. The ESRF and the NWO are acknowledged for allocating beam time at the Dutch-Belgian beamline (DUBBLE) for the GIWAXS experiments. The

ferroelectric measurements have been conducted at the ELOR-PrintTec Platform (ANR-10-EQPX-28-01/Equipex ELORPrintTec).

Appendix A. Supplementary data

Supplementary data related to this article can be found at https://doi.org/10.1016/j.polymer.2018.06.072.

References

[1] A.J. Lovinger, Ferroelectric polymers, Science 220 (4602) (1983) 1115–1121.
[2] R.C.G. Naber, C. Tanase, P.W.M. Blom, G.H. Gelinck, A.W. Marsman, F.J. Touwslager, S. Setayesh, D.M. De Leeuw, High-performance solution-processed polymer ferroelectric field-effect transistors, Nat. Mater. 4 (3) (2005) 243–248.
[3] K. Asadi, D.M. De Leeuw, B. De Boer, P.W.M. Blom, Organic non-volatile memories from ferroelectric phase-separated blends, Nat. Mater. 7 (7) (2008) 547–550.
[4] R.C.G. Naber, K. Asadi, P.W.M. Blom, D.M. De Leeuw, B. De Boer, Organic nonvolatile memory devices based on ferroelectricity, Adv. Mater. 22 (9) (2010) 933–945.
[5] K. Asadi, M. Li, N. Stingelin, P.W.M. Blom, D.M. De Leeuw, Crossbar memory array of organic bistable rectifying diodes for nonvolatile data storage, Appl. Phys. Lett. 97 (2010) 193308.
[6] A.J. Lovinger, G.T. Davis, T. Furukawa, M.G. Broadhurst, Crystalline forms in a copolymer of vinylidene fluoride and trifluoroethylene (52/48 mol %), Macromolecules 15 (2) (1982) 323–328.
[7] A.J. Lovinger, Ferroelectric transition in a copolymer of vinylidene fluoride and tetrafluoroethylene, Macromolecules 16 (9) (1983) 1529–1534.
[8] K. Tashiro, K. Takano, M. Kobayashi, Y. Chatani, H. Tadokoro, Structural study on ferroelectric phase transition of vinylidene fluoride-trifluoroethylene copolymers (III) dependence of transitional behavior on VDF molar content, Ferroelectrics 57 (1) (1984) 297–326.
[9] H. Tanaka, H. Yukawa, T. Nishi, Effect of crystallization condition on the ferroelectric phase transition in vinylidene fluoride/trifluoroethylene (VF2/F3E) copolymers, Macromolecules 21 (8) (1988) 2469–2474.
[10] J.F. Legrand, Structure and ferroelectric properties of P(VDF-TrFE) copolymers, Ferroelectrics 91 (1) (1989) 303–317.
[11] K. Tashiro, M. Kobayashi, Structural phase transition in ferroelectric fluorine polymers: X-ray diffraction and infrared/Raman spectroscopic study, Phase Transitions 18 (3–4) (1989) 213–246.
[12] K.J. Kim, G.B. Kim, C.L. Vanlencia, J.F. Rabolt, Curie transition, ferroelectric crystal structure, and ferroelectricity of a VDF/TrFE(75/25) copolymer 1. The effect of the consecutive annealing in the ferroelectric state on curie transition and ferroelectric crystal structure, J. Polym. Sci. B Polym. Phys. 32 (15) (1994) 2435–2444.
[13] K.J. Kim, G.B. Kim, Curie transition, ferroelectric crystal structure and ferroelectricity of a VDF/TrFE (75/25) copolymer: 2. The effect of poling on curie transition and ferroelectric crystal structure, Polymer 38 (19) (1997) 4881–4889.
[14] E. Bellet-Amalric, J.F. Legrand, Crystalline structures and phase transition of the ferroelectric P(VDF-TrFE) copolymers, a neutron diffraction study, Eur. Phys. J. B 3 (2) (1998) 225–236.
[15] E.B. Gowd, N. Shibayama, K. Tashiro, Structural correlation between crystal lattice and lamellar morphology in the phase transitions of uniaxially oriented syndiotactic polystyrene (δ and δe forms) as revealed by simultaneous measurements of wide-angle and small-angle x-ray scatterings, Macromolecules 41 (7) (2008) 2541–2547.
[16] F. Bargain, P. Panine, F. Domingues Dos Santos, S. Tencé-Girault, From solvent-cast to annealed and poled poly(VDF-co-TrFE) films: new insights on the defective ferroelectric phase, Polymer 105 (2016) 144–156.
[17] Y. Tajitsu, H. Ogura, A. Chiba, T. Furukawa, Investigation of switching characteristics of vinylidene fluoride/trifluoroethylene copolymers in relation to their structures, Jpn. J. Appl. Phys. 26 (4 R) (1987) 554–560.
[18] Z.-G. Zeng, G.-D. Zhu, L. Zhang, X.-J. Yan, Effect of crystallinity on polarization fatigue of ferroelectric P(VDF-TrFE) copolymer films, Chin. J. Polym. Sci. 27 (04) (2009) 479–485.
[19] D. Mao, M.A. Quevedo-Lopez, H. Stiegler, B.E. Gnade, H.N. Alshareef, Optimization of poly(vinylidene fluoride-trifluoroethylene) films as non-volatile memory for flexible electronics, Org. Electron. 11 (5) (2010) 925–932.
[20] D. Guo, I. Stolichnov, N. Setter, Thermally induced cooperative molecular reorientation and nanoscale polarization switching behaviors of ultrathin poly(vinylidene fluoride-trifluoroethylene) films, J. Phys. Chem. B 115 (46) (2011) 13455–13466.
[21] R. Mahdi, W. Gan, W. Majid, Hot plate annealing at a low temperature of a thin ferroelectric P(VDF-TrFE) film with an improved crystalline structure for sensors and actuators, Sensors 14 (10) (2014) 19115.
[22] A. Aliane, M. Benwadih, B. Bouthinon, R. Coppard, F. Domingues-Dos Santos, A. Daami, Impact of crystallization on ferro-, piezo- and pyro-electric characteristics in thin film P(VDF-TrFE), Org. Electron. 25 (2015) 92–98.
[23] J. Kim, J.H. Lee, H. Ryu, J.-H. Lee, U. Khan, H. Kim, S.S. Kwak, S.-W. Kim, High-performance piezoelectric, pyroelectric, and triboelectric nanogenerators based on P(VDF-TrFE) with controlled crystallinity and dipole alignment, Adv. Funct. Mater. 27 (22) (2017) 1700702.
[24] W. Xia, Z. Wang, J. Xing, C. Cao, Z. Xu, The dependence of dielectric and ferroelectric properties on crystal phase structures of the hydrogenized P(VDF-TrFE) films with different thermal processing, IEEE Trans. Ultrason. Ferroelectrics Freq. Contr. 63 (10) (2016) 1674–1680.
[25] A.J. Lovinger, G.E. Johnson, H.E. Bair, E.W. Anderson, Structural, dielectric, and thermal investigation of the Curie transition in a tetrafluoroethylene copolymer of vinylidene fluoride, J. Appl. Phys. 56 (9) (1984) 2412–2418.
[26] P. Sharma, T.J. Reece, S. Ducharme, A. Gruverman, High-resolution studies of domain switching behavior in nanostructured ferroelectric polymers, Nano Lett. 11 (5) (2011) 1970–1975.
[27] M.A. Barique, H. Ohigashi, Annealing effects on the Curie transition temperature and melting temperature of poly(vinylidene fluoride/trifluoroethylene) single crystalline films, Polymer 42 (11) (2001) 4981–4987.
[28] D. Zhao, I. Katsouras, K. Asadi, P.W.M. Blom, D.M. De Leeuw, Switching dynamics in ferroelectric P(VDF-TrFE) thin films, Phys. Rev. B Condens. Matter Mater. Phys. 92 (21) (2015) 214115.
[29] K. Koga, H. Ohigashi, Piezoelectricity and related properties of vinylidene fluoride and trifluoroethylene copolymers, J. Appl. Phys. 59 (6) (1986) 2142–2150.
[30] Y.J. Park, S.J. Kang, C. Park, K.J. Kim, H.S. Lee, M.S. Lee, U.-I. Chung, I.J. Park, Irreversible extinction of ferroelectric polarization in P(VDF-TrFE) thin films upon melting and recrystallization, Appl. Phys. Lett. 88 (24) (2006) 242908.
[31] F. Xia, B. Razavi, H. Xu, Z.-Y. Cheng, Q.M. Zhang, Dependence of threshold thickness of crystallization and film morphology on film processing conditions in poly(vinylidene fluoride–trifluoroethylene) copolymer thin films, J. Appl. Phys. 92 (6) (2002) 3111–3115.
[32] Z. Fu, W. Xia, W. Chen, J. Weng, J. Zhang, J. Zhang, Y. Jiang, G. Zhu, Improved thermal stability of ferroelectric phase in epitaxially grown P(VDF-TrFE) thin films, Macromolecules 49 (10) (2016) 3818–3825.
[33] W. Bras, I.P. Dolbnya, D. Detollenaere, R. van Tol, M. Malfois, G.N. Greaves, A.J. Ryan, E. Heeley, Recent experiments on a small-angle/wide-angle X-ray scattering beam line at the ESRF, J. Appl. Crystallogr. 36 (3 Part 1) (2003) 791–794.
[34] P. Müller-Buschbaum, The active layer morphology of organic solar cells probed with grazing incidence scattering techniques, Adv. Mater. 26 (46) (2014) 7692–7709.
[35] G. Renaud, R. Lazzari, F. Leroy, Probing surface and interface morphology with grazing incidence small angle x-ray scattering, Surf. Sci. Rep. 64 (8) (2009) 255–380.
[36] K. Koga, N. Nakano, T. Hattori, H. Ohigashi, Crystallization, field-induced phase transformation, thermally induced phase transition, and piezoelectric activity in P(vinylidene fluoride-TrFE) copolymers with high molar content of vinylidene fluoride, J. Appl. Phys. 67 (2) (1990) 965–974.
[37] R. Hasegawa, Y. Takahashi, Y. Chatani, H. Tadokoro, Crystal structures of three crystalline forms of poly(vinylidene fluoride), Polym. J. 3 (5) (1972) 600–610.
[38] A.J. Lovinger, T. Furukawa, G.T. Davis, M.G. Broadhurst, Crystallographic changes characterizing the Curie transition in three ferroelectric copolymers of vinylidene fluoride and trifluoroethylene: 1. As-crystallized samples, Polymer 24 (10) (1983) 1225–1232.
[39] T. Furukawa, Ferroelectric properties of vinylidene fluoride copolymers, Phase Transitions 18 (3–4) (1989) 143–211.
[40] R. Gregorio, M.M. Botta, Effect of crystallization temperature on the phase transitions of P(VDF/TrFE) copolymers, J. Polym. Sci. B Polym. Phys. 36 (3) (1998) 403–414.
[41] K. Tashiro, R. Tanaka, Structural correlation between crystal lattice and lamellar morphology in the ferroelectric phase transition of vinylidene fluoride–trifluoroethylene copolymers as revealed by the simultaneous measurements of wide-angle and small-angle X-ray scatterings, Polymer 47 (15) (2006) 5433–5444.
[42] Q. Guo, Polymer Morphology: Principles, Characterization, and Processing, Wiley, 2016.